Materials Chemistry and Physics 133 (2012) 932–940

Contents lists available at SciVerse ScienceDirect

Materials Chemistry and Physics

journal homepage: www.elsevier.com/locate/matchemphys

Modeling porosity of high surface area nanopowders of the gallium nitride GaN semiconductor

Mariusz Drygas, Jerzy F. Janik*

Faculty of Energy and Fuels, AGH University of Science and Technology, Al. Mickiewicza 30, 30-059 Krakow, Poland

ARTICLE INFO

Article history:
Received 28 October 2011
Received in revised form 25 January 2012
Accepted 28 January 2012

Keywords:
Nitrides
Powder diffraction
Adsorption
Surface properties
Computer modeling and simulation

ABSTRACT

A pool of high surface area gallium nitride GaN nanopowders was prepared and suitably characterized. The powders appeared to be mostly mesoporous with increasing share of microporosity at the highest surface area end. The BET surface area values spanned the range from 6.3 $m^2 g^{-1}$ to 222 $m^2 g^{-1}$ and specific mesopore volumes reached up to 0.21 $cm^3 g^{-1}$. Powder XRD scans indicated for all samples the hexagonal polytype of GaN. Average crystallite sizes were calculated from the XRD data with Scherrer equation. Helium pycnometry was used to determine skeletal densities of the nanopowders in the wide range of 3.6–6.1 $g cm^{-3}$. The densities showed an evident particle size dependence that could be explained by the presence of specific crystallite agglomerates impenetrable by helium atoms. Herein, a simple model of porosity for nanocrystalline powders, specifically nano-GaN, is proposed and confronted with the experimental data. The surface area for such nanopowders was modeled with appropriately specified surfaces of close-packed spheres (rigid and non-rigid configurations) as a function of sphere diameter. Selected model variants were statistically best-fitted with experimental data points, *i.e.*, BET specific surface areas and average crystallite sizes determined from the XRD scans, to yield very good solutions. They support the view that the BET surface area of the GaN nanocrystalline powders basically corresponds with the accessible surface area of the nanoparticles – crystallites and/or agglomerates.

© 2012 Elsevier B.V. All rights reserved.

1. Introduction

In our quest for the optimization of non-additive high temperature/high pressure sintering of GaN nanopowders [1] where surface properties play an important role as well as in the rare porosity related studies of such powders, both reported by us [2] and others [3], one is faced with an intriguing observation. Namely, the maximum BET surface areas for the well-defined GaN nanocrystalline materials are found in the relatively low and narrow range spanning from a few to up to *ca.* 200–300 $m^2 g^{-1}$. Furthermore, our numerous efforts to prepare powders with yet higher surface areas *via* several synthesis methods have repeatedly failed to succeed. Given the available data on GaN porosity, it is tempting to suggest that there could likely be more fundamental reasons for the observed BET surface area limitations than mere experimental circumstances.

Similar to the above or smaller BET values, typical for mesoporosity (2–50 nm pore diameters, according to IUPAC), were also reported for the nanopowders of other metal nitrides such as AlN [2a,4], TiN [5], VN [6], and various non-oxide materials of apparent nanocrystallinity [7]. This had to be contrasted with certain nitrides prepared from polymeric precursors of which surface areas reached much higher levels as was the case of Si_3N_4 [8] – up to the 1000 $m^2 g^{-1}$ range and BN [9] – up to the 1400 $m^2 g^{-1}$ range. Significantly, those silicon nitride materials were reported to be amorphous while the boron nitride materials showed the turbostratic structure of highly disordered nature paralleling the isostructural graphite and, therefore, both these nitrides can hardly be classified as "typical" nanocrystalline powders with distinct crystallites. They rather constitute a specific class of porous bodies with structural features resembling those of many amorphous carbons with prevailing microporosity and resulting extremely high total surface areas that reach for the latter the values in the 4000 $m^2 g^{-1}$ or even higher range [10].

In summary of this aspect, it has become customary for materials scientists to include the BET surface area, S_{BET} [$m^2 g^{-1}$], as an indispensable part of surface characterization of many if not all high surface area solids. This versatile yet equivocally interpreted parameter has even become standardized by IUPAC, presently including both micro- and mesoporous solids [11]. Briefly, the method involves the determination of the amounts of the adsorbate, usually nitrogen gas at its boiling point, adsorbed on accessible surfaces at various relative pressures. Then, the monolayer-related surface area can be calculated from the adsorption isotherm by means of the BET equation [12]. It appears that despite cautious arguing by adsorptionists the method provides useful characterization parameters both for amorphous materials with a characteristic

* Corresponding author.
E-mail address: janikj@agh.edu.pl (J.F. Janik).

0254-0584/$ – see front matter © 2012 Elsevier B.V. All rights reserved.
doi:10.1016/j.matchemphys.2012.01.119

net of propagating pores (*e.g.*, carbons – coal adsorbents, silica gels) or crystalline materials with a well-defined inner pore structure (*e.g.*, zeolites, molecular sieves). However, neither of these cases can be directly related to nanocrystalline powders consisting physically of non-porous crystallites, possibly, in either rigid or non-rigid arrangements. In this regard, some earlier reports have suggested that a pore structure modeled by regularly packed spherical particles could well represent a certain type of porosity [13] which, in our view, may be relevant to many nanocrystalline solids.

These observations made us look for another readily available characterization method possibly providing independent results on porosity that could be related to the BET data. In this regard, it has become standard in materials science that the powder X-ray diffraction (XRD) method is applied for structure elucidations of crystalline materials including nanopowders. In addition to structural details, the XRD data provide with a means to estimate an average crystallite diameter by using the Scherrer equation [14]. In fact, there is a great deal of controversy about the "true" meaning of a such-derived crystallite dimension but at least for a pool of related materials it constitutes a reliable parameter of choice for comparison purposes [15]. This has proved true so many times despite the obvious fact that in reality we deal with particle size distributions. In this regard, excluding the case of purposedly made 1-D and 2-D nanostructures, it happpens frequently in the domain of nanosized crystalline particles that their shapes and sizes are relatively uniform with yet no preferential direction of growth clearly established. Supporting evidence for this kind of situation is ocassionally provided by both scanning and transmission microscopy. Since the average crystallite size *via* the Scherrer equation is conveniently derived from the XRD structure studies, it is used in practice more often than any of the size-related parameters from microscopical studies [16].

Herein, we report a study which to the best of our knowledge is, for the first time, aimed at modeling a specific surface area in nanocrystalline powders, specifically, nanocrystalline gallium nitride powders. The theoretical model variants include close-packed equidimensional spheres in rigid and non-rigid arrangements for which gas accessible surfaces are shown to be definite functions of a sphere diameter. Parallely, a pool of twelve GaN nanopowders with the XRD-derived average crystallite diameters, D_{GaN}, spanning the range from 1 to 39 nm was synthesized and suitably characterized including determinations of the BET surface area to confront the size/surface properties of the samples with the model. The choice of the XRD (particle size) and BET (surface area) methods for model verification was done primarily because of their common applications in materials characterization. The helium density determinations were used to probe an extent of gas impenetrable particle agglomeration having an essential impact on model refinement. The appropriate model-related characterization of the samples was complemented with the examples of typical SEM and TEM images.

2. Experimental

2.1. Sample preparation

Total 12 GaN nanopowders were synthesized to span the 1–39 nm crystallite diameter range. Seven materials with the smallest crystallite sizes in the 1.0–8.1 nm range were prepared with our anaerobic synthesis method by pyrolysis of gallium imide [17], *i.e.*, samples (gas atmosphere/pyrolysis temperature in °C/pyrolysis time in hours): 1 – vacuum/450/4, 2 – N_2/450/4, 3 – NH_3/350/4, 4 – NH_3/450/4, 5 – NH_3/600/4, 6 – NH_3/700/4, 7 – NH_3/800/16. Four materials with the intermediate to large crystallite sizes, 17.0–30.0 nm range, were made with a two-step aerosol-assisted method by nitridation of gallium nitrate starting from its solutions in various solvents [18], *i.e.*, samples (solvent/pyrolysis temperature in °C/pyrolysis time in hours): 8 – DMF + methanol/950/12, 9 – DMF/950/12, 10 – methanol/950/12, 11 – water/975/6. Finally, one material, *i.e.*, sample 12 with the largest crystallite size of 39.0 nm was obtained by nitriding pyrolysis of gallium oxide Ga_2O_3 powder under an ammonia flow at 950 °C for 12 h [18a].

2.2. Characterization

The sample structures were determined by standard powder XRD spectroscopy (X'Pert Pro Panalytical with Cu K_α source; 2Θ = 20–80°). All diffraction patterns are available as Supplementary material. Average crystallite sizes were evaluated from Scherrer equation applying the Rietveld refinement method [14]. For the evaluation, changes of the line profile parameters compared to a standard sample were utilized. Our standard was a polycrystalline alumina sintered body with an average grain size over 5 μm subjected to stress relief annealing. The profile parameters depend on the instrument settings used for data collection and on the profile function used for the refinement. In our analysis the full Voight function was used to describe the profile of the measured diffraction lines. The total profile width is a convolution of the Gaussian profile part and of the Lorentzian profile part and these parts are combined numerically. In such a method, the full width at half-maximum (*fwhm*) is only one of a few fitted parameters. Average crystallite sizes for a few powders with the smallest particle sizes and severely defected hexagonal lattices were simply evaluated from the fwhm of their very broad lines [19]. Helium densities were obtained by Micromeritics AccuPyc. Standard 5-point BET surface areas, mesopore volumes, and average mesopore diameter (the latter two based on BJH theory applied to the desorption part of the isotherm hysteresis) were determined by low temperature nitrogen adsorption on Micromeritics Gemini 2380. Prior the adsorption determinations, the samples were heat-conditioned under dynamic vacuum at 300 °C for 1 h. SEM images were acquired with a Hitachi Model S-4700 scanning electron microscope. TEM observations were carried out on a JEOL JEM 3010 electron microscope operating at an accelerating voltage of 300 kV.

3. Results

3.1. Basic properties of nanopowders

The characteristics of the GaN nanopowders are shown in Table 1. The samples from 1 to 12 are listed according to the increasing average crystallite diameter from 1.0 to 39.0 nm. As will be shown later, this size range covers the essential properties of the model within the surface area *vs.* sphere diameter coordinates.

One has to acknowledge that despite the meticulous procedure applied to calculate the average crystallite diameters, D_{GaN}, these values represent merely decent approximations. This is due to inherent constraints of the Scherrer eguation but, mainly, because estimations of even such common parameters as average crystallite sizes and lattice parameters can be seriously misinterpreted for nanopowders if standard calculation tools that have been derived for microcrystalline systems are applied [15]. We are acutely aware of this problem that may introduce a rather undefined error in the calculated crystallite sizes. Having said that, we decided to use the XRD-derived average crystallite diameter as the reference particle dimension mainly due to its convenient determination and widespread use. In this regard, our model assumes averaging out crystallite sizes *via* supposing equidimentional spheres and, therefore, the XRD average crystallite size seems to be quite an adequate reference point to confront the model with the experimental data.

Table 1
Average crystallite sizes (D_{GaN}), helium densities (D_{He}), BET surface areas (S_{BET}), mesopore volumes (V_{meso}), and average mesopore diameters (BJH/des) determined for the nanocrystalline GaN powders.

Sample no.	D_{GaN} (XRD) [nm]	D_{He} [g cm^{-3}]	S_{BET} [m^2 g^{-1}]	V_{meso} (BJH/des) [cm^3 g^{-1}]	Av. pore size (BJH/des) [nm]
1	1.0	3.6	179	0.021	2.7
2	1.2	3.8	165	0.089	2.4
3	1.6	4.0	134	0.070	3.7
4	1.8	4.5	222	0.138	2.6
5	3.0	5.2	103	0.154	4.6
6	6.0	5.2	58	0.146	6.9
7	8.1	5.0	42	0.143	17.8
8	17.0	6.0	23.5	0.181	19.0
9	18.0	6.0	24.0	0.213	20.3
10	18.0	6.1	20.8	0.086	15.1
11	30.0	6.0	6.3	0.015	11.5
12	39.0	6.1	8.0	0.019	11.6

All this means that we consciously simplified the problem of particle size distribution for the sake of simplicity of the model, at least, at this stage of model development.

The typical TEM and SEM micrographs of the selected GaN nanopowders are shown in Figs. 1 and 2, respectively. In Fig. 1, the TEM images for two powders prepared by the anaerobic route display similar morphologies of quite regularly shaped and uniformly-sized crystallites some of them showing up as apparent aggregates of superimposed translucent particles that is characteristic for such TEM measurements. Here, deciphering particle size details requires a tedious shade-differing particle contour analysis best performed on original images. In 2–3 times enlarged rectangular parts of the pictures, some tightly bound agglomerates can also be seen (*e.g.*, in the encircled areas, groups of densely packed crystallites). In Fig. 2, the SEM images taken for a typical powder from the aerosol-assisted synthesis bring out the initial spheroidal morphology of the raw powder. Upon the final nitriding treatment the large spheres turn evidently to the assemblages of small crystallites, similarly, as earlier discussed for the anaerobic route materials, of quite uniform size and shape. Some tightly bound crystallite agglomerates can also be seen upon magnification (micrograph on the right-hand side). At this point, we want to make a distinction between the particles loosely packed in aggregates and the particles tightly bound in agglomerates. For the latter, we will concentrate on GaN particle assemblages that are impenetrable by such probing gas entities as helium atoms (helium density measurements) and nitrogen molecules (BET determinations). In general, the microscopical sizes of crystallites in both cases correspond reasonably well with the respective average crystallite sizes calculated from the Scherrer equation.

The BET surface areas for the powders span the range from 6.3 to 222 m^2 g^{-1}. Based on the BJH analysis, the powders are mostly mesoporous while those with the smallest crystallite sizes show also some microporosity (some pores with sizes < 2 nm). The highest mesopore volumes of *ca.* 0.20 cm^3 g^{-1} that are accompanied by the largest average pore diameters of approx. 20 nm are determined for Samples 8 and 9 prepared by the aerosol-assisted synthesis utilizing the organic solvent solutions of the precursor.

3.2. Variability of helium density

The essential observation in this study is concerned with the significant variation of helium densities among the powders, *i.e.*, from 3.6 to 6.1 g cm^{-3}, to be compared with the crystalline density of 6.1 g cm^{-3} for hexagonal GaN [20]. In this regard, we estimate that possible impact on density of both the specific properties of GaN nanocrystallites (differences in lattice constants between the surface layer and core) and structural defects could not account for more than some 5–10% of discrepancies to be compared with the observed largest relative decrease of density of *ca.* 40%. In other words, there has to be yet another factor siginificantly contributing to the phenomenon. Such a factor should account for a definite relationship between the density and crystallite size, D_{GaN}, as shown by the scatter plot in Fig. 3 (solid diamonds).

This experimental trend can be understood in terms of a certain number of GaN crystallites forming a tight agglomerate with distances between them smaller than the size of He atoms used to probe the density (agglomerate mostly impenetrable for helium). The image on the left hand side in Fig. 3 shows an idealized spherical assemblage of smaller spherical particles separated by 0.26 nm, the so-called kinetic diameter of He that is frequently used in gas adsorption studies [21] while in several instances He atom diameters in the 0.18–0.24 nm range are quoted as well [22]. The density of such an agglomerate is derived in the top equation while its changes with diameter are shown as a solid line in the accompanying graph. There are also two other solutions/lines shown there, *i.e.*, for He atom diameters of 0.20 nm and 0.30 nm.

In our opinion, this represents a surprisingly good match between the helium density experimental data and the theoretical predictions based on the derived equation for He atom diameters in the 0.20–0.26 nm range and, therefore, providing strong arguments for the presence of helium impenetrable agglomerates of GaN crystallites. As a consequence, this puts a definite constraint on the interpretation of gas adsorption data in this system and, likely, in many similar nanocrystalline systems since the crystallite diameter from XRD data may not match the particle diameter sensed by an adsorbing gas. From a materials chemist point of view, the formation of such agglomerates can be envisioned as resulting from multi-center crystallization within an initial particle of the precursor during its conversion to the nitride.

4. Modeling specific surface area

4.1. Model variants

We considered three model variants of porosity in the nanocrystalline gallium nitride system each of them assuming equidimensional spherical particles (crystallites or crystallite agglomerates) in a close-packed arrangement while allowing for non-rigidity of particles with respect to adsorbed nitrogen molecules (Figs. 4–7). Each of the model variants relates a specific surface area of particles (as accessed by adsorbed nitrogen molecules in a monolayer *via* the sitting area of N_2) and particle diameter and is solved for two options, *i.e.*, one that assumes the sitting area of 0.162 nm^2 for a single adsorbed N_2 molecule on a flat surface (S [m^2 g^{-1}]) and another that includes a correction for the sitting area of a N_2 molecule adsorbed on a curved surface of a sphere (S_{corr} [m^2 g^{-1}]). Graph *d* in the lower right-hand corner in Fig. 4 is intended to explain the applied correction k for such a surface curvature effect that is equally valid for all the variants. Graphs *a–c* show schematically the relevant geometrical relations, consecutively, in model variants 1–3 that are used to derive the model equation for the specific surface area S in each case. The density of particles is expressed by the formula shown in Fig. 3 for the crystalline agglomerates. All the formulae are derived assuming the helium atom diameter of 0.26 nm and the commonly accepted nitrogen molecule diameter of 0.455 nm. The relevant calculations, specifically, for model variant 1 as an example are shown in Fig. 5. The number of particles in 1 cm^3 for the close-packed arrangement

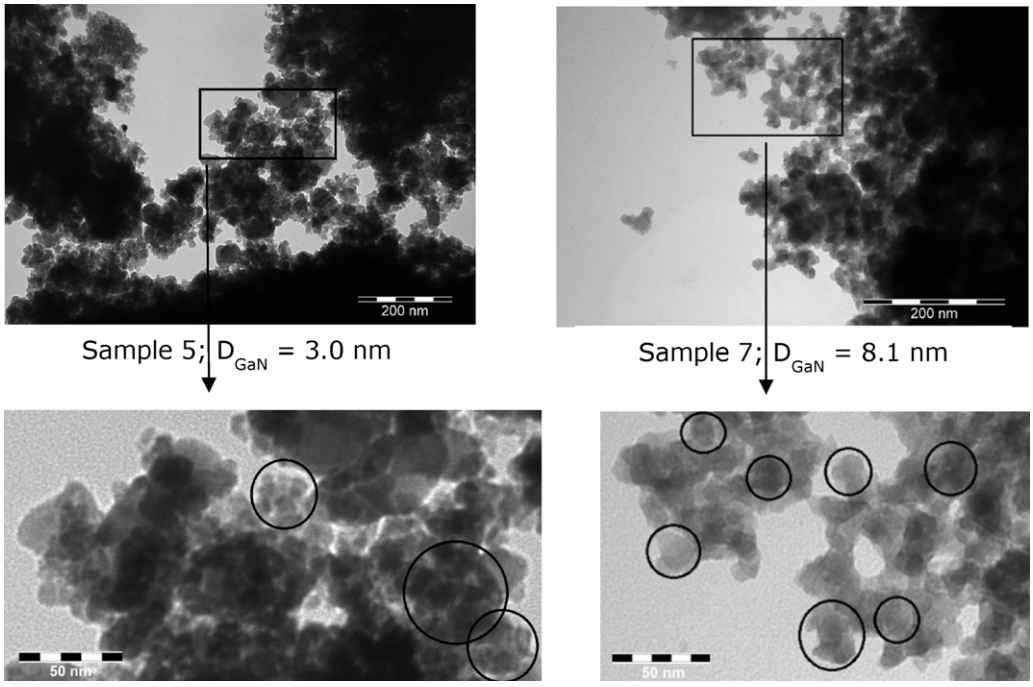

Fig. 1. TEM pictures of Sample 5 (left) and Sample 7 (right) from the anaerobic synthesis of GaN nanopowders. The circles in the enlarged areas tentatively point out to crystallite agglomerates.

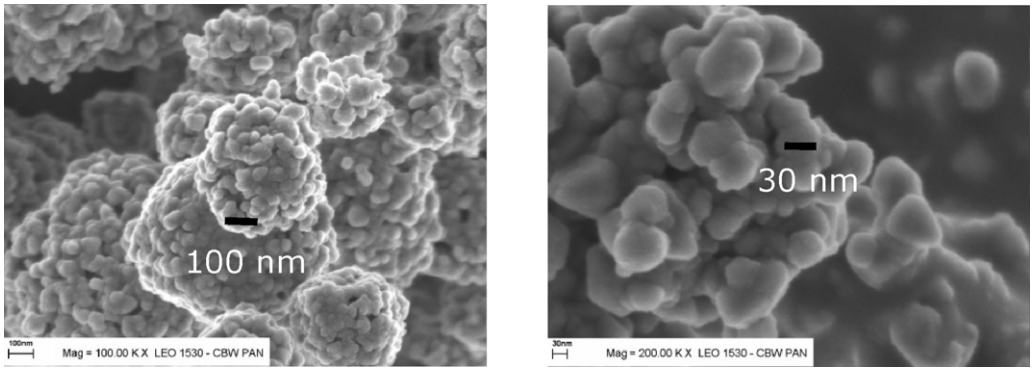

Fig. 2. SEM images of Sample 11 from the aerosol-assisted synthesis of GaN nanopowders.

$$d_{aggl}\ [g/cm^3] = \frac{m_{aggl}}{V_{aggl}} = 6.1\frac{n\cdot\frac{4}{3}\pi(\frac{D_{GaN}}{2})^3}{n\cdot\frac{4}{3}\pi(\frac{D_{GaN}+D_{He}}{2})^3} = 6.1\frac{D_{GaN}^{\ 3}}{(D_{GaN}+D_{He})^3} = \boxed{6.1\frac{D_{GaN}^{\ 3}}{(D_{GaN}+0.26)^3}}$$

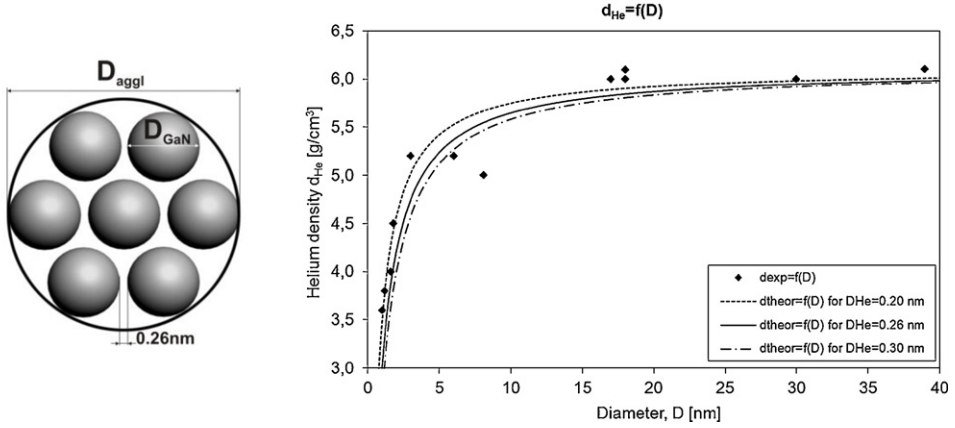

Fig. 3. The experimental (diamonds) and theoretical (lines) relationships between helium density and particle diameter; the theoretical curves are calculated for the agglomerate as shown on the left and defined by the equation on top for D_{He} (solid line for D_{He} = 0.26 nm).

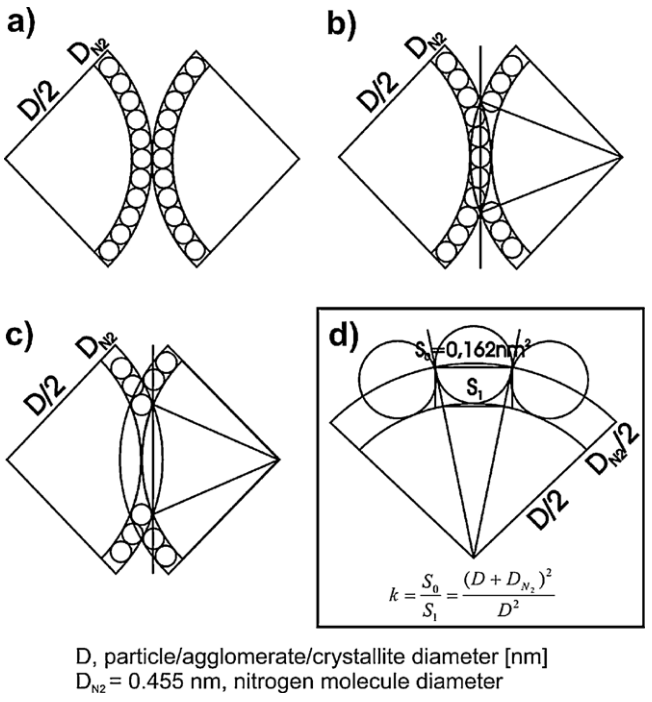

Fig. 4. Geometrical relations in model variants 1, 2, and 3 used for the derivation of model equations (*a*, *b*, and *c*, respectively) and N_2 sitting area correction parameter *k* (*d*).

of spheres, n/cm^3, is obtained by dividing 0.7405 (part of the volume occupied by spheres in the close-packed system) by the normalized volume of one sphere which in this case has a diameter of $D+2D_{N2}$ (D – diameter of solid nanoparticle, nm; D_{N2} – diameter of nitrogen molecule, nm). The surface area in m^2 of a single solid nanoparticle, S_p, is calculated as for a sphere. The total surface area of spheres in 1 cm^3, S [$m^2\,cm^{-3}$], is then obtained as a product of the number of particles and the surface area of a single particle. Finally, such a surface area is divided by density as derived in Fig. 3 to yield the commonly used specific surface area, S [$m^2\,g^{-1}$]. This value is further multiplied by k – correction for surface curvature as explained in Fig. 4d resulting in the corrected specific surface area, S_{corr} [$m^2\,g^{-1}$]. The final solutions for the specific surface areas are shown in the boxes.

In Figs. 5–7, included are graphical representations of model variants with the derived relationships within the specific surface area/particle diameter coordinates together with the experimental data points (scatter plots), *i.e.*, BET surface area *vs.* D_{GaN}, the latter determined from the Scherrer equation. At this point, we note that the abscissa for the model relationships is tied to a general particle/agglomerate diameter D while for the experimental data points it is tied to a crystallite diameter D_{GaN} which, in a general case, means that these axes may not overlap.

4.2. Model adjustments and experimental verification

Since the particle diameter probed by an adsorbing gas, in general, does not have to be equivalent to the crystallite diameter (from XRD data) we assume, in the first approach, that the particle diameter D in the model equations, except for the term associated with helium density, can be expressed as a product, $a\,D_{GaN}$, with the parameter a to be best-fitted by the least-square method applied to the experimental data points. In the second approach, we also suppose that the constant of 728.36 that is derived by assuming the equidimensional spheres in an ideal close-packed arrangement can be "relaxed" and is taken as a second variable, b, in the fit. This, in

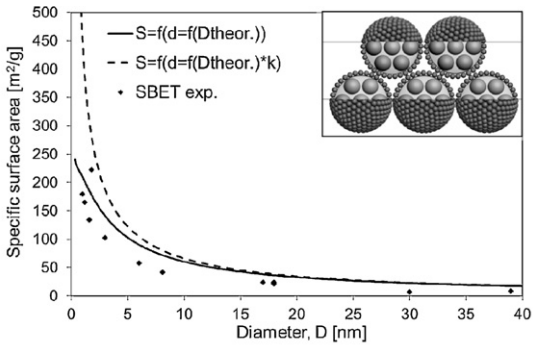

$$n/cm^3 = \frac{0.7405}{\frac{4}{3}\pi(\frac{D+2D_{N_2}}{2})^3 \cdot 10^{-21}};\ \text{n - number of particles per 1 cm}^3$$

$$S_p\,[m^2] = 4\pi(\frac{D}{2})^2 \cdot 10^{-18};\ \text{S}_\text{p}\text{ - particle surface area}$$

$$S\,[m^2/cm^3] = n \cdot S_p = \frac{0.7405}{\frac{4}{3}\pi(\frac{D+2D_{N_2}}{2})^3 \cdot 10^{-21}} \cdot 4\pi(\frac{D}{2})^2 \cdot 10^{-18} = \frac{4443 \cdot D^2}{(D+2D_{N_2})^3}$$

$$S\,[m^2/g] = \frac{4443 \cdot D^2}{(D+2D_{N_2})^3} \cdot \frac{(D+D_{He})^3}{6.1 \cdot D^3} = \frac{728.36 \cdot D^2}{(D+2D_{N_2})^3} \cdot \frac{(D+D_{He})^3}{D^3}$$

$$S_{corr}\,[m^2/g] = S\,[m^2/g] \cdot k = \frac{728.36 \cdot (D+D_{N_2})^2}{(D+2D_{N_2})^3} \cdot \frac{(D+D_{He})^3}{D^3}$$

Fig. 5. Model variant 1 – double adsorbate molecule layer particle bridging.

physical sense, accommodates for averaging out some deviations from such an assumption. Finally, the remaining constant value in model variants 2 and 3 is tried as the third variable, c. As a consequence, up to three otherwise fixed parameters that result from suitable model assumptions are relaxed to become best-fitted variables while the overall mathematical expressions of the models stay unchanged. The best-fit calculations use the pairs of the experimental BET surface areas, S_{BET}, and crystallite diameters from XRD scans, D_{GaN}.

Note that the equations for variant 1 do not intrinsically have the variable c. Fig. 8 as an example presents the fitted equations for the case of no correction for the cross-sectional area of N_2 for model variant 2. The starting model equation on top can be compared

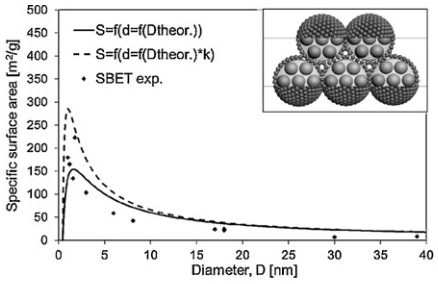

$$S\,[m^2/g] = (D^2 - \frac{3 \cdot D^2 \cdot D_{N_2}}{D+2D_{N_2}}) \cdot \frac{728.36}{(D+D_{N_2})^3} \cdot \frac{(D+D_{He})^3}{D^3}$$

$$S_{corr}\,[m^2/g] = S\,[m^2/g] \cdot k = (1 - \frac{3 \cdot D_{N_2}}{D+2D_{N_2}}) \cdot \frac{728.36}{(D+D_{N_2})} \cdot \frac{(D+D_{He})^3}{D^3}$$

Fig. 6. Model variant 2 – single adsorbate molecule layer particle bridging.

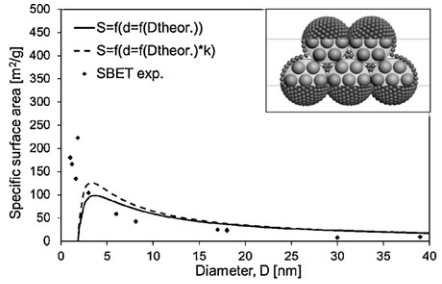

$$S\,[m^2/g] = \left(1 - \frac{6D_{N_2}}{D + 2D_{N_2}}\right) \cdot \frac{728.36}{D} \cdot \frac{(D + D_{He})^3}{D^3}$$

$$S_{corr}\,[m^2/g] = S\,[m^2/g] \cdot k = \left(1 - \frac{6D_{N_2}}{D + 2D_{N_2}}\right) \cdot \frac{728.36 \cdot (D + D_{N_2})^2}{D^3} \cdot \frac{(D + D_{He})^3}{D^3}$$

Fig. 7. Model variant 3 – no adsorbate molecule layer particle bridging.

with a particular best-fitted equation below and all three "relaxed" variables can be identified. Similar procedures were applied for all other model variants.

5. Discussion

The correlation coefficients *R*'s found for the best-fitted equations are collected in Table 2 in which, tentatively, we underlined the selected *R*'s for the best and simplest solutions and attached below them the best-fitted values of *a* and *b*. Overall, we find very good solutions for each of the model variants supported by the high values of *R* reaching 0.95 in each case. However, the simplest solution with *R* equal 0.95 appears to be for model variant 2 with no correction for the cross-sectional area of N_2 and with only one fitted parameter *a* (*a* = 1.42). It is worth pointing out that despite purely statistical data treatment all the fitted values of *a* are larger than one, possibly, supporting the constant's physical significance that can be linked to an averaged agglomerate size as defined by the expression $a{\cdot}D_{GaN}$ for particle diameter in the equations. In a few cases, especially for model variant 3, we find that the application of the correction for the cross-sectional area of N_2 yields comparatively good results (*e.g.*, one fitted parameter *a* = 2.47, *R* = 0.94), however, at the expense of a relatively more complicated equation.

The high *R*-values of the order of 0.94–0.95 for all three model variants describe, however, somewhat different variability trends

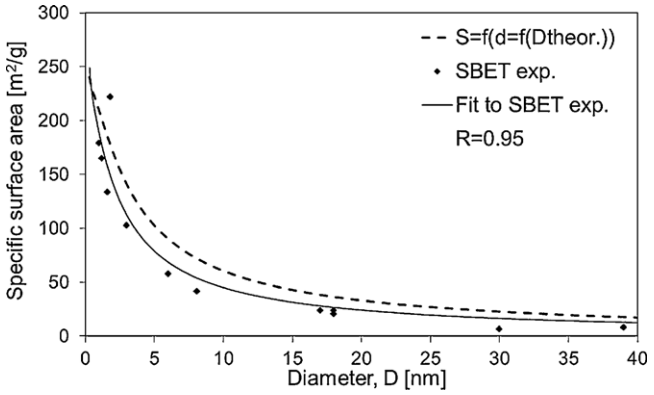

Fig. 9. Model variant 1 with no correction for cross-sectional area of N_2 – theoretical model curve (dashed line), scatter plot (diamonds), best-fit curve (solid line) with two adjusted variables *a*, *b*, and correlation coefficient *R* = 0.95.

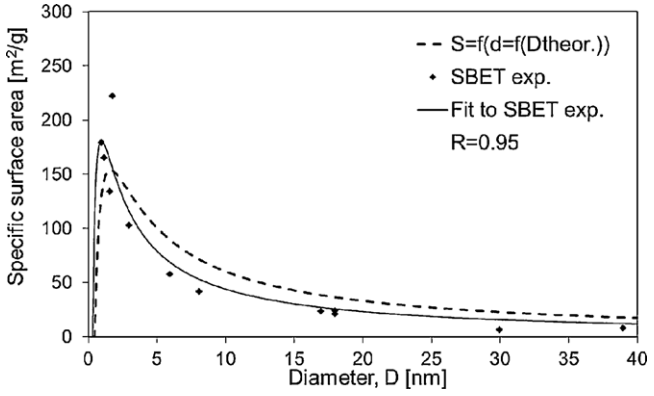

Fig. 10. Model variant 2 with no correction for cross-sectional area of N_2 – theoretical model curve (dashed line), scatter plot (diamonds), best-fit curve (solid line) with a single adjusted variable *a*, and correlation coefficient *R* = 0.95.

as illustrated in Figs. 9–11 for the selected best solutions in model variants 1, 2, and 3, consecutively, and in Fig. 12 for the second equally good solution for model variant 3 (the solutions that are underlined in Table 2). Each of the figures includes the scatter plot as the background for the theoretical model variant curve (dashed line) and best-fitted curve (solid line).

The solutions in model variant 1 (Fig. 9) are characteristic of a continuous and steep increase of both curves for $D < ca.$ 3 nm.

(i) *No correction* for the cross-sectional area of N_2

$$S\,[m^2/g] = \left(1 - \frac{6 \cdot D_{N_2}}{D + 2D_{N_2}}\right) \cdot \frac{728.36}{D} \cdot \frac{(D + D_{He})^3}{D^3}$$

a – relaxed variable (relaxed D)

$$S\,[m^2/g] = \left(1 - \frac{6 \cdot D_{N_2}}{a \cdot D + 2D_{N_2}}\right) \cdot \frac{728.36}{a \cdot D} \cdot \frac{(D + D_{He})^3}{D^3}$$

a, b – relaxed variables (relaxed D and one "constant")

$$S\,[m^2/g] = \left(1 - \frac{6 \cdot D_{N_2}}{a \cdot D + 2D_{N_2}}\right) \cdot \frac{b}{a \cdot D} \cdot \frac{(D + D_{He})^3}{D^3}$$

a, b, c – relaxed variables (relaxed D and two "constants")

$$S\,[m^2/g] = \left(1 - \frac{c \cdot D_{N_2}}{a \cdot D + 2D_{N_2}}\right) \cdot \frac{b}{a \cdot D} \cdot \frac{(D + D_{He})^3}{D^3}$$

Fig. 8. Model variant 2 – the black arrows point to the equations best-fitted to experimental data (the case of no correction for the cross-sectional area of N_2).

Table 2
Correlation coefficients R's and relevant *a*, *b* values for best-fitted model variants.

	Model variant 1			Model variant 2			Model variant 3		
	Only *a*	*a* and *b*	*a*, *b*, and *c*	Only *a*	*a* and *b*	*a*, *b*, and *c*	Only *a*	*a* and *b*	*a*, *b*, and *c*
Correction for cross-sectional area of N_2									
Yes	0.84	0.94	n/a	0.65	0.95	0.93	0.94 *a* = 2.47	0.95	0.95
No	0.91	0.95 *a* = 1.18 *b* = 615.8	n/a	0.95 *a* = 1.42	0.95	0.95	0.88	0.95 *a* = 2.58 *b* = 987.4	0.95

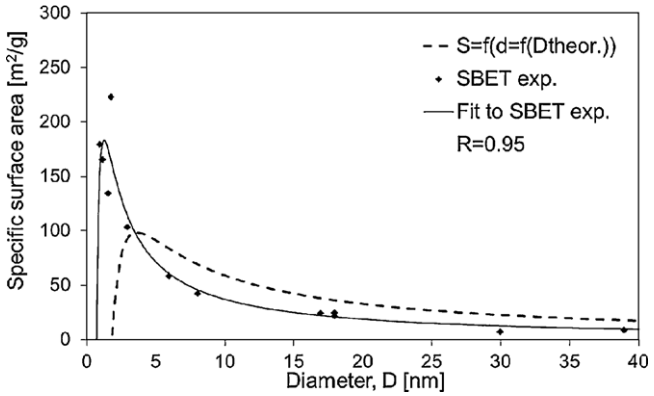

Fig. 11. Model variant 3 with no correction for cross-sectional area of N_2 – theoretical model curve (dashed line), scatter plot (diamonds), best-fit curve (solid line) with two adjusted variable *a*, *b*, and correlation coefficient $R = 0.95$.

Practically, for the smallest particle diameters of the order of 1 nm, the predicted values of the surface area S are not exceeding 200–230 $m^2\ g^{-1}$. By best-fitting *a* and *b* in the initial model relationship (dashed line), the resulting curve (solid line) matches better the apparent trend of the scatter plot throughout the entire range of particle diameter.

Model variant 2 (Fig. 10) shows a distinctly different trend than discused above that is exemplified by the initial (dashed line) and the best-fitted (solid line) curves, namely, there is a clear maximum at *D* *ca.* 1.5–2.0 nm and 1.0–1.5 nm on these curves, respectively. The maximum predicted value of *S* on the initial curve reaches 150 $m^2\ g^{-1}$ and on the best-fitted curve closes up at some 180 $m^2\ g^{-1}$. It is worth noting that the scatter plot actually provides some arguments for a similar experimental data point variability as predicted by this model variant. In this regard, the highest surface area of 222 $m^2\ g^{-1}$ is found for a GaN powder with $D = 1.8$ nm but there are three powders with *D* smaller than 1.8 nm that show

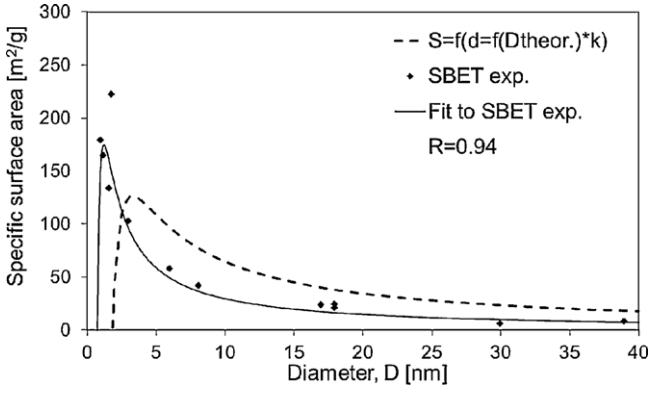

Fig. 12. Model variant 3 with correction for cross-sectional area of N_2 – theoretical model curve (dashed line), scatter plot (diamonds), best-fit curve (solid line) with a single adjusted variable *a*, and correlation coefficient $R = 0.94$.

lower specific surface areas than that while for *D* values larger than 1.8 nm the data points nicely follow the smooth descent of both model curves. In this case, best-fitting of only one parameter *a* appears to yield a better match with the scatter plot than approximated by the initial model curve. We want to stress, however, that the inherent uncertainty of the XRD-derived average crystallite diameter in a few nanometer range is rather high and does not accurately support the discussed trend below *ca.* 2 nm. We are simply faced here with intrinsic limitations of the XRD method and Scherrer equation as applied to nanocrystalline powders. Despite these circumstances, we believe that the applied consistent methodologies of the XRD size and BET surface area determinations warrant sufficient credibility for the overall trend and magnitudes of the particle size/surface area ranges.

The general variability trend in model variant 3 with no correction for the cross-sectional area of N_2 is qualitatively similar to the previous case (Fig. 11). This model predicts a maximum surface area *S* of some 100 $m^2\ g^{-1}$ for *D* at *ca.* 3–4 nm (dashed line). However, in the best-fitted curve with two adjusted parameters, *i.e.*, *a* and *b* (solid line), the maximum is moved to smaller *D*'s at *ca.* 1.5 nm with the corresponding value of S reaching approx. 180 $m^2\ g^{-1}$. Again, the best-fitted curve follows the scatter plot closer than the initial model curve does. The equally good solution with a similar variability trend for this model variant is obtained for the version with the cross-sectional area of N_2 and the best-fit with a single adjusted parameter *a* (Fig. 12).

Although, most of the selected tentative best solutions encompass the options with no correction for the cross-sectional area of N_2 (relatively simple solutions), one has to note that by including such a correction the resulting curves yield in principle higher values of *S* for a given *D* (Figs. 5–7) and, for instance, in the realm of initial model variant 2 the then-predicted maximum values of *S* are in the 280–290 $m^2\ g^{-1}$ range for *D* of *ca.* 1.0–1.5 nm (Fig. 6). These values of specific surface area appear to constitute the upper range of BET surface areas reported to date for many nanocrystalline nitrides including GaN [2–7].

Based on the discussion above, we suppose that model variant 2 with a single adsorbant layer particle bridging describes the BET results satisfactorily and in the most consistent way. However, higher values of *S* determined for some samples compared with the predictions of this variant would suggest that the situation somewhat between model variants 1 and 2 describes the system even more adequately. Alternatively, comparable good/simple results are obtained for model variant 3 with no adsorbate molecule layer particle bridging, especially, when applying the correction for the cross-sectional area of N_2. We want to underline here that despite a lack of a clear-cut situation about the best solution, all the variants are consistent in the magnitudes of the surface area in relation to the experimental data and, therefore, support the outer surface of nanoparticles (nanocrystallites and/or nanoagglomerates) to constitute the specific surface area determined by the BET method.

A challenging task is posed now as to an experimental discrimination between the two essentially different model options with

plausible important implications. It is worth to recall that the first option (models variants 1 and 2) assumes that the particles, *i.e.*, GaN tight agglomerates or nanocrystallites or both do form a relatively loosely aggregated system that allows for particle displacement upon interactions with adsorbing nitrogen molecules. This option yields good matches with the experimental data without considering the correction for the sitting area of N_2. The second option (model variant 3) of a more conservative nature provides with equally satisfactory results by assuming that the system does not allow for particle displacement during adsorption and, additionally, requires taking into consideration the reasonable correction for the cross-sectional area of N_2.

We want to stress that the satisfactory model solutions are obtained for the broad range of powders with the crystallite sizes from 1.0 to 39.0 nm despite the inherent uncertainties associated with the determination of crystallite diameter for nanosized materials *via* standard powder XRD data work-up. These uncertainties are especially pronounced for the nanopowders with the smallest crystallite sizes of the order of a few nanometers with severely defected lattices. In this regard, we believe that the implementation of a consistent procedure including both XRD determinations and follow-up calculations of the crystallite size is a key to a successful application of the model for various nanocrystalline powders.

We also want to add that equally satisfactory results are obtained with all model variants when used for the Langmuir surface area *vs.* particle size relationships (topic not explored in this report). All this leads us to think that such good correlations of the adsorption data with the models that assume, somewhat simplistically, the BET/Langmuir surface areas as resulting from monolayer capacity of the system is a strong argument for relating, in fact, these parameters to the surface area of crystallite agglomerates and crystallites. We plan further work on the application of the models to specific surface areas and pore volumes derived from the BJH data to confirm the models general relevance to modeling porosity in such nanocrystalline systems.

It seems conceivable that for other size/shape homogeneous nanocrystalline powders the basic idea of the present study will also be true, *i.e.*, the specific surface area can be shown to be directly linked to the outer particle surface of a crystallite or gas-impenetrable agglomerate. Moreover, we think that upon suitable model modifications it can also be applied to various well-defined non-equidimensional particle systems such as nanorods, nanotubes, and nanosheets. The helium density measurements may become essential along the way for evaluating gas penetrability in the agglomerates or within the specific volumes like those inside the nanotubes. Further elaboration of this simple and realistic approach for nanopowders would greatly help in the interpretation of standard gas adsorption data and, for instance, one could estimate chances for getting some microporosity equivalence in a nanocrystalline system of interest.

6. Conclusions

The analysis of the three model variants of close-packed equidimensional spheres as feasible particle systems for nanocrystalline GaN powders provides strong arguments for linking the experimental BET surface area with the outer surface of the nanoparticles. The nanoparticles are made of regularly shaped crystallites or crystallite agglomerates with the size of the latter being a definite function of the constituent crystallite diameter. The statistical best-fit of the initial model relationships and the experimental data points including BET surface area, S_{BET}, and average crystallite size from XRD determinations, D_{GaN}, yields satisfactory approximations that can be used, for instance, to forecast the specific surface area of the nanopowders from crystallite size determinations or interpret the spatial circumstances behind the formally determined micro- and mesoporosity. This is true independent on the underlying assumptions concerned with the physical aspects of the three model options. The helium density measurements proved to provide the essential information about the presence of gas impenetrable agglomerates. The challenging questions that arise from this study of the possible non-rigid nanoparticle configurations/swelling under adsorption conditions and/or plausible significance of N_2 molecule adsorption on curved surfaces of extremely small particles are prompting us for further adsorption studies in this nitride system.

Acknowledgement

Research supported by the Polish Ministry of Science and Higher Education/MNiSW, Grant no. N N 507 443534. Fruitful discussions with Prof. Leszek Czepirski and Prof. Miroslaw M. Bucko from AGH-UST are highly appreciated. We are grateful to Tomasz Miotk (student) for his help with computer graphics.

Appendix A. Supplementary data

Supplementary data associated with this article can be found, in the online version, at doi:10.1016/j.matchemphys.2012.01.119.

References

[1] (a) S. Stelmakh, A. Swiderska-Sroda, G. Kalisz, S. Gierlotka, E. Grzanka, B. Palosz, M. Drygas, J.F. Janik, R.T. Paine, Proceedings of the International Conference on Nanoscience and Technology, Basel, Switzerland, July 30 to August 4, 2006, Institute of Physics Publishing, Philadelphia, PA, 2006, p. 1399;
(b) E. Grzanka, S. Stelmakh, S. Gierlotka, A. Swiderska-Sroda, G. Kalisz, B. Palosz, M. Drygas, J.F. Janik, R.T. Paine, European Powder Diffraction Conference, EPDIC-10, Geneva, Switzerland, September 1–4, 2006;
(c) J. Borysiuk, P. Caban, W. Strupinski, S. Gierlotka, S. Stelmakh, J.F. Janik, Cryst. Res. Technol. 42 (2007) 1291;
(d) M. Drygas, Z. Olejniczak, E. Grzanka, M.M. Bucko, R.T. Paine, J.F. Janik, Chem. Mater. 20 (2008) 6816;
(e) M. Drygas, M.M. Bucko, Z. Olejniczak, I. Grzegory, J.F. Janik, Mater. Chem. Phys. 122 (2010) 537.
[2] (a) L. Czepirski, J.F. Janik, E. Komorowska-Czepirska, R.L. Wells, Adsorpt. Sci. Technol. 20 (2002) 723;
(b) M. Drygaś, J.F. Janik, L. Czepirski, Mater. Res. Bull. (2011), submitted.
[3] (a) G. Chaplais, S. Kaskel, J. Mater. Chem. 14 (2004) 1017;
(b) C. West, R. Mokaya, Chem. Mater. 21 (2009) 4080.
[4] (a) For example, see: J.-H. Pee, J.-C. Park, K.-T. Hwang, S.R. Kim, W.-S. Cho, Res. Chem. Intermed. 36 (2010) 801;
(b) G.J. Yan, G.D. Chen, B.K.L. Jiang, Y.L. Wu, Mater. Lett. 63 (2009) 2205;
(c) A.-J. Chang, S.-W. Rhee, S. Baik, J. Mater. Sci. 31 (1996) 5701.
[5] (a) For example, see: I.-S. Kim, P.N. Kumta, J. Mater. Chem. 13 (2003) 2028;
(b) S. Kaskel, K. Schlichte, G. Chaplais, M. Khanna, J. Mater. Chem. 13 (2003) 1496;
(c) M. Drygas, C. Czosnek, R.T. Paine, J.F. Janik, Chem. Mater. 18 (2006) 3122;
(d) J.H. Bang, K.S. Suslick, Adv. Mater. 21 (2009) 3186;
(e) S. Dong, X. Chen, L. Gu, X. Zhou, H. Xu, H. Wang, Z. Liu, P. Han, J. Yao, L. Wang, G. Cui, L. Chen, ACS Appl. Mater. Interfaces 3 (2011) 93.
[6] (a) For example, see: R. Kapoor, S.T. Oyama, J. Solid State Chem. 9 (1992) 303;
(b) H. Kwon, S. Choi, L.T. Thompson, J. Catal. 184 (1999) 236.
[7] R.W. Charley, P.W. Lednor, Adv. Mater. 3 (1991) 474.
[8] (a) S. Kaskel, K. Schlichte, J. Catal. 201 (2001) 270;
(b) S. Kaskel, K. Schlichte, B. Zibrowius, Phys. Chem. Chem. Phys. 4 (2002) 1675;
(c) K. Luyjew, N. Tonanon, V. Pavarajarn, J. Am. Ceram. Soc. 91 (2008) 1365.
[9] (a) J.F. Janik, W.C. Ackerman, R.T. Paine, D.-W. Hua, A. Maskara, D.M. Smith, Langmuir 10 (1994) 514;
(b) G.L. Wood, R.T. Paine, Chem. Mater. 18 (2006) 4716.
[10] J. Lee, J. Kim, T. Hyeon, Adv. Mater. 18 (2006) 2073.
[11] (a) ISO 9277:2010, Determination of the Specific Surface Area of Solids by Gas Adsorption – BET Method, second edition, ISO 9277, ISO, Geneva, 2010;
(b) K.S.W. Sing, D.H. Everett, R.A.W. Haul, L. Moscou, R.A. Pierotti, J. Rouquerol, T. Siemieniewska, Reporting physical adsorption data for gas/solid systems with special reference to the determination of surface area and porosity (IUPAC Recommendations 1984), Pure Appl. Chem. 57 (1985) 603.
[12] S. Brunauer, P.H. Emmett, E. Teller, J. Am. Chem. Soc. 60 (1938) 309.
[13] (a) D.D. Dollimore, G.R. Heald, J. Colloid Interface Sci. 42 (1973) 233;
(b) D.C. Havard, R. Wilson, J. Colloid Interface Sci. 57 (1976) 276.
[14] P.H. Klug, E.L. Alexander, in X-ray Diffraction Procedures, John Wiley & Sons, New York, 1974.

[15] (a) B. Palosz, E. Grzanka, S. Gierlotka, S. Stel'makh, R. Pielaszek, W. Lojkowski, U. Bismayer, J. Neuefeind, H.P. Weber, W. Palosz, Phase Transit. 76 (2003) 171;
(b) V. Petkov, M. Gateshki, J. Choi, E.G. Gillan, Y. Ren, J. Mater. Chem. 15 (2005) 4654;
(c) U. Tamas, J. Gubicza, Z. Kristallogr. 222 (2007) 114.
[16] (a) For example, see: B. Schwenzer, J. Hu, D.E. Morse, Adv. Mater. 23 (2011) 2278;
(b) M. Lei, H.Z. Zhao, H. Yang, P.G. Li, H.L. Tang, B. Song, W.H. Tang, Diam. Relat. Mater. 16 (2007) 1974;
(c) P.G. Li, M. Lei, Y.X. Du, X. Guo, W.H. Tang, Appl. Surf. Sci. 255 (2009) 3843;
(d) L. Jia, E.Q. Xie, X.J. Pan, Z.X. Zhang, Y.Z. Zhang, Mater. Sci. Technol. 25 (2009) 1498;
(e) H. Qiu, C. Cao, H. Zhu, Mater. Sci. Eng. B 136 (2007) 33.
[17] (a) J.F. Janik, R.L. Wells, Chem. Mater. 8 (1996) 2708;
(b) R.L. Wells, J.F. Janik, W.L. Gladfelter, J.L. Coffer, M.A. Johnson, B.D. Steffey, Mater. Res. Soc. Symp. Proc. 468 (1997) 39;
(c) J.F. Janik, R.L. Wells, J.L. Coffer, J.V. St. John, W.T. Pennington, G.L. Schimek, Chem. Mater. 10 (1998) 1613.
[18] (a) G.L. Wood, E.A. Pruss, R.T. Paine, Chem. Mater. 13 (2001) 12;
(b) J.F. Janik, M. Drygas, S. Stelmakh, E. Grzanka, B. Pałosz, R.T. Paine, Phys. Status Solidi A 203 (2006) 1301.
[19] (a) For example, see: J.-W. Hwang, J.P. Campbell, J. Kozubowski, S.A. Hanson, J.F. Evans, W.L. Gladfelter, Chem. Mater. 7 (1995) 517;
(b) J.A. Jegier, S. McKernan, A.P. Purdy, W.L. Gladfelter, Chem. Mater. 12 (2000) 1003.
[20] M. Levinshtein, S. Rumyantsev, M. Shur, Properties of Advanced Semiconductor Materials, Wiley, New York, 2001.
[21] V. Boffa, J.E. ten Elshof, A.V. Petukhov, D.H.A. Blank, ChemSusChem 1 (2008) 437.
[22] E.V. Kalashnikov, B.Z. Pevzner, Phys. Solid State 44 (2002) 294.